Chinese Chemical Letters 33 (2022) 767–772

Contents lists available at ScienceDirect

Chinese Chemical Letters

journal homepage: www.elsevier.com/locate/cclet

Let-7i miRNA and platinum loaded nano-graphene oxide platform for detection/reversion of drug resistance and synergetic chemical-photothermal inhibition of cancer cell

Jianhua Yan[a], Yixuan Zhang[a], Lijuan Zheng[a], Yuwei Wu[a], Ting Wang[a], Ting Jiang[b], Xiaoqin Liu[b], Dongming Peng[c], Yanfei Liu[b,*], Zhenbao Liu[a,d,*]

[a] *Department of Pharmaceutics, Xiangya School of Pharmaceutical Sciences, Central South University, Changsha 410013, China*
[b] *Department of Pharmaceutical Engineering, College of Chemistry and Chemical Engineering, Central South University, Changsha 410083, China*
[c] *Department of Medicinal Chemistry, School of Pharmacy, Hunan University of Chinese Medicine, Changsha 410208, China*
[d] *Molecular Imaging Research Center of Central South University, Changsha 410008, China*

ARTICLE INFO

Article history:
Received 11 June 2021
Revised 3 August 2021
Accepted 5 August 2021
Available online 11 August 2021

Keywords:
Nano-graphene oxide
Drug resistance
Synergetic chemical-photothermal therapy
miRNA
Platinum

ABSTRACT

The drug resistance of chemotherapy is a major challenge to overcome for antineoplastic agents and the reverse of drug resistant is essential for cancer therapy. Herein, we developed a drug delivery system which can simultaneously detect/reverse the drug resistance and perform synergetic treatment of cancer. In this work, we integrated cyanine5 (Cy5) modified miRNA (*let-7i*) (Cy5-miRNA) and platinum onto nano-graphene oxide (NGO) (30-50 nm) platform to achieve simultaneously detection/reversion of drug resistance and synergetic treatment of cisplatin resistant $SKOV_3$ cells ($SKOV_3$DDP cells). The Cy5-miRNA adsorbed on NGO could selectively bind the drug resistance related mRNA follow by suppress the expression of drug resistance mRNA, and the binding simultaneously induced the release of Cy5-miRNA from the NGO, thus the fluorescence signal of Cy5 recovered and could be used for drug resistance monitoring. Moreover, the miRNA suppressed the Cyclin D1 protein expressions thus reversed the drug resistance. The loaded platinum(IV) (Pt(IV)) was converted to the therapeutic platinum(II) (Pt(II)) in both tumor acidic and reductive environment responsive behavior. NGO furtherly performed photothermal therapy under near infrared (NIR) laser irradiation and enhanced the therapeutic effect. All in all, this nanoplatform realized detection/reversion of the drug resistance as well as synergetic chemical-photothermal treatment of ovarian cancer cells, which holds great promise in the treatment of drug resistant cancer cells.

Platinum, a common chemotherapeutic drug for treatment of cancer [1,2], shows high anti-cancer property [3]. However, it has tumor drug resistance and side effects [4]. Drug resistance is a typical phenomenon during cancer treatment, especially the platinum induced resistance, which is the major barrier for cisplatin-based chemotherapy [5]. The mechanisms of cisplatin related resistance involve over expression of drug resistant related mRNA [6,7]. miRNAs, a class of non-protein-coding endogenous RNAs with ~22 bp, can partially complementarily bind to the 3′-untranslated regions of the target mRNA, resulting in the degradation of mRNA to inhibit the express of protein [8,9]. *Let-7* family, one of tumor drug resistance suppressor miRNAs [10,11], shows binding and inhibition abilities towards target mRNA. There is increasing evidence that the *let-7* family can negatively regulate multiple proteins, such as rat sarcoma (Ras), high mobility group A2 (HMGA2), c-Myc, definition cell division cycle 25A (CDC25A), cyclin-dependent kinases (CDK6), Cyclin D2 [12-14]. It was reported that up-regulating the expression of *let-7i* effectively reversed cisplatin resistance in patients with epithelial ovarian cancer [15], thus delivery *let-7i* miRNA into drug resistant cancer cells would be a promising strategy to reverse the drug resistance.

Recently drug delivery systems and biosensors based on nanomaterials [16-21], especially graphene oxide (GO) have attracted great attentions contributed to rich functional groups and high loading efficiency of molecules *via* π-π stacking [22,23]. The adsorption of GO with ssDNA has been utilized to selection of high affinity aptamers [24]. In addition, biosensors based on GO and fluorophore modified nucleic acid have been utilized for intercellular molecules diagnosis [16,25]. We previously established a aptamer/GO probe for intercellular ATP specific detection [22]. Here,

* Corresponding authors.
E-mail addresses: liuyf@csu.edu.cn (Y. Liu), zhenbaoliu@csu.edu.cn (Z. Liu).

https://doi.org/10.1016/j.cclet.2021.08.018
1001-8417/

employing fluorophore modified *let-7i* miRNA can be used as a probe to detect the drug resistant related mRNA thus to monitor the drug resistance degree. Meanwhile, loading miRNAs on GO could be a promising strategy for drug resistance reverse, which has seldom been reported. To reduce off-target toxicity of drugs, the nanocarrier was functionalized by folate for targeting factor [26]. Besides, tumor microenvironment responsive release of drug has attracted increasing attention recently [18], molecules linked to the GO could be designed to release drug in tumor microenvironment responsive behavior. Moreover, GO has photothermal conversion ability [27], which could be used for photothermal treatment of cancer, thus simultaneous reverse drug resistance and synergetic chemical-photothermal inhibition of cancer could be achieved based on miRNA/GO system.

Herein, in this study, we loaded cyanine5 (Cy5) modified miRNA (*let-7i*) and Pt(IV) into PEGylated nano-graphene oxide (NGO-PEG) platform to reverse drug resistance of epithelial ovarian cancer cells ($SKOV_3$ cells) and inhibit cancer cells in a chemical-photothermal synergetic manner. Folate was modified on to this platform to achieve targeted delivery into drug resistant cancer cells. miRNA (*let-7i*) was adsorbed onto the NGO, and it could be desorbed from NGO due to forming miRNA-mRNA double strand complex through partially complementary binding to the intracellular mRNAs. The miRNA-mRNA complex could be release from NGO and fluorescence of Cy5 will be recovered for drug resistance mRNA detection. Besides, delivery of *let-7i* into cancer cells could be used for inhibition the expression of mRNA thus reversing the chemo-resistance. Pt(IV) is linked to the PEG which was modified on the surface of GO, and Pt(IV) could be reduced into Pt(II) under the stimuli of glutathione (GSH) in the cancer intracellular microenvironment. In addition, graphene oxide could be used for photothermal treatment of cancer. All in all, this platform is expected to achieve enhanced therapeutic efficacy through reversion of drug resistance and synergetic chemical-photothermal inhibition of ovarian cancer cells.

First, Pt(IV)-COOH was synthesized and characterized. Fig. 1A shows the synthetic route of the preparation of Pt(IV)-COOH. The synthesis of Pt(IV) was began with cisplatin. H_2O_2 was used to introduce two hydroxyl groups on cisplatin. Then the products were reacted with succinic anhydride to form Pt(IV)-COOH with a free carboxyl group capable of reacting with NH_2 group in the 4-arm-NH_2-PEG. Fig. 1B showed the FTIR spectra of cisplatin, Pt(IV)-OH and Pt(IV)-COOH. Pt(IV)-OH displayed peaks at 3520 cm^{-1} and 540 cm^{-1}. The Pt(IV)-COOH showed peaks at 1702 cm^{-1} and 1645 cm^{-1}, which were free carboxyl group and coordinated carboxyl group, respectively. ^1H NMR (DMSO-d_6) results showed the data of δ 6.50 (6H), 2.4-2.3 (4H) (Fig. S1 in Supporting information). As indicated by the mass spectrum, the major peak at *m/z* 432.96 (Fig. S2 in Supporting information) could be attributed to the deprotonated Pt(IV)-COOH. The results all indicated the successful synthesis of Pt(IV)-COOH.

Then GO, NGO and $^{cy5\text{-}miR}$NGO-PEG-FA-Pt were synthesized and characterized. AFM images indicated the commercialized crude GO (Fig. S3 in Supporting information) has single-layer structure and the size was about 200-500 nm and sickness was around 0.8 nm. The size of prepared NGO (Fig. S4 in Supporting information) was much smaller, which was about 30-50 nm, the sickness was 0.8-1.0 nm, which were satisfactory to meet the requirements as a drug carrier. The size of ^{miR}NGO-PEG-FA-Pt (Fig. 1E) was about 50-60 nm, the sickness was about 2 nm, which were attributed to the modifications. Raman spectra in Fig. S5 (Supporting information) showed that the NGO owned higher intensity of the D/G ratio and D peak than that of GO, illustrating the carboxyl groups and edge structures were formed during cleavage. The synthesis of PEG-FA was monitored by HPLC (Fig. S6 in Supporting information). The retention time of free FA, activated FA and PEG-FA were 6.3, 8.3 and 16 min, respectively. The longer retention time of PEG-FA than that of FA was due to the conjugation of PEG and FA. FT-IR spectrum (Fig. 1C) indicated that NGO displayed a peak at 1730 cm^{-1}, which could be attributed to the carboxyl group. After coating PEG-FA onto NGO, carboxylic group of NGO peak at 1730 cm^{-1} disappeared and two new characteristic peaks at 1642 cm^{-1} and 1457 cm^{-1} appeared, which could be attributed to the -CONH amide band I and C-N stretching vibration, respectively. The UV-vis spectrum (Fig. 1D) of NGO-PEG-FA revealed that the peak at 233 nm disappeared and a new peak at 272 nm appeared, indicating the presence of PEG-FA in the NGO-PEG-FA. The characteristic peaks of PEG-FA had a blue shift, indicating the modification of NGO with PEG-FA. These results all indicated the success synthesis of NGO-PEG-FA. In addition, thermogravimetric analysis (TGA) (Fig. S7 in Supporting information) was used to characterize the mass fraction of PEG-FA in NGO-PEG-FA. For NGO, a slow weight loss at 100 °C and an accelerated weight loss at 150 °C were observed, which could be attributed to the absorbed water and carboxylic groups, respectively. For PEG-FA, the quick weight loss at around 300 °C was due to the decomposition of PEG in the PEG-FA. The TGA results showed that the mass fraction of PEG-FA in NGO-PEG-FA was about 96.9%. The loading of Pt(IV)-COOH onto NGO-PEG-FA was confirmed by ICP-OES. And the Pt(IV) content of NGO-PEG-FA-Pt was determined to be about 6%. The amount of Cy5-miRNA adsorbed on NGO-PEG-FA was illustrated in Fig. S8 (Supporting information), NGO effectively quenched the fluorescence of Cy5, indicating the absorption of miRNA onto NGO. The results indicated that 200 μg/mL NGO-PEG-FA adsorbed 500 nmol/L Cy5-miRNA totally.

To gain the photothermal performance of NGO and NGO-PEG-FA-Pt, 20-80 μg/mL of NGO-PEG-FA-Pt or NGO was irradiated with 808 nm laser at 1.5 W/cm^2 for 10 min. The temperature was recorded (Fig. 2A). The results indicated that the temperature of the PBS solution remained at 25-28 °C, while 80 μg/mL of NGO-PEG-FA-Pt and NGO gradually reached 57.9 °C and 52.8 °C, respectively. To investigate the photothermal stability, the NGO-PEG-FA-Pt and NGO solution (80 μg/mL) was irradiated with 808 nm laser for 10 min, followed by switching off the NIR laser and cooling to room temperature. Photothermal reproducibility of NGO-PEG-FA-Pt and NGO (Fig. 2B) was displayed. Fig. 2C showed that both NGO-PEG-FA-Pt and NGO showed good dispersion and stability in water, MES, PBS, and cell medium for two weeks. No aggregation was observed.

Drug release behaviors of NGO-PEG-FA-Pt was further investigated in reductive conditions such as intracellular glutathione (GSH). GSH was thus used to trigger the release of Pt from NGO-PEG-FA-Pt. PBS solutions (pH 7.4, GSH 5 μmol/L) and (pH 5.0, GSH 5 mmol/L) were used to imitate the physiological environment and tumor intracellular environment, respectively. The results in Fig. 2D indicated that almost 90% of Pt(II) was released in 24 h in the condition of (pH 5.0, GSH 5 mmol/L), while in the condition of (pH 7.4, GSH 5 μmol/L), the drug released much slower and only ~63% drug was released even after 24 h. Thus NGO-PEG-FA-Pt released drug in responsive to acid and reductive environment, which could be used for tumor environment triggered drug release.

To detect the drug resistant related intracellular mRNA, the $^{Cy5\text{-}miR}$NGO-PEG-FA was incubated with $SKOV_3$ and $SKOV_3$DDP cells. As illustrated in Fig. 3A, obvious stronger red fluorescence was observed in the $SKOV_3$DDP cells compared with the $SKOV_3$ cells both in 30 min and 2 h, the fluorescence signal was due to the released Cy5-miRNA from the nanosheets after binding with the target mRNA and recovered the fluorescence signal, the results indicated that a higher drug resistance-related target mRNA expression in $SKOV_3$DDP cells was observed. The relative fluorescence signals in $SKOV_3$ and $SKOV_3$DDP cells were measured and illustrated in Fig. S9 (Supporting information). The relative fluo-

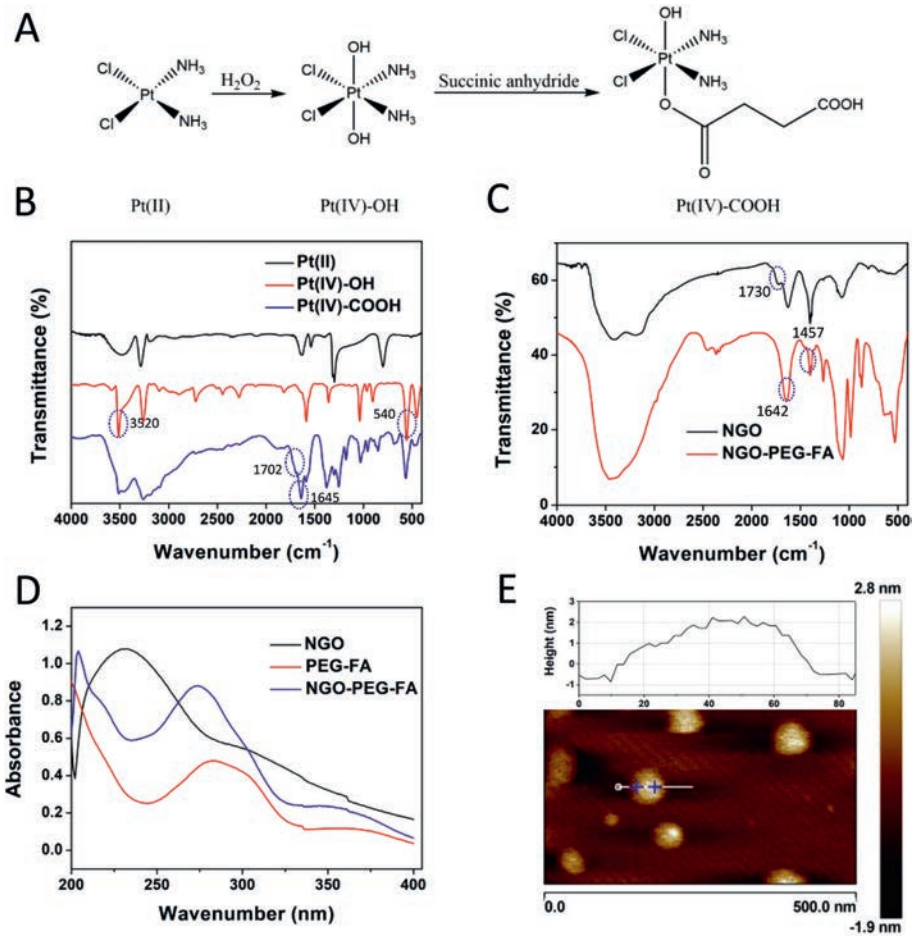

Fig. 1. (A) The synthetic route of Pt(IV)-COOH. (B) FT-IR spectra of Pt(II), Pt(IV)-OH and Pt(IV)-COOH. (C) FT-IR spectra of NGO, NGO-PEG-FA. (D) UV spectra of NGO, PEG-FA and NGO-PEG-FA. (E) AFM images of $^{Cy5\text{-}miR}$NGO-PEG-FA-Pt.

rescence signals in $SKOV_3$DDP cells to be 2.1 and 17.5 at 30 min and 2 h, respectively, while in $SKOV_3$ cells, it was 0.2 and 4.5 at 30 min and 2 h, respectively, indicating the drug resistance related mRNA in $SKOV_3$DDP cells is about 4 folds of the level in $SKOV_3$ cells in 2 h treatment. Through comparing the fluorescence signal in $SKOV_3$DDP cells and $SKOV_3$ cells, the drug resistance degree could be determined. We then compared this method with traditional tedious MTT assay for drug resistance measurement. We measured the drug resistance index of $SKOV_3$DDP cells using MTT assay through comparing the IC_{50} of Pt(II) to $SKOV_3$ and $SKOV_3$DDP cells. As shown in Fig. S10 (Supporting information), Pt(II) displayed dose-dependent cytotoxicity towards both $SKOV_3$ and $SKOV_3$DDP cells from 1 μmol/L to 64 μmol/L. The IC_{50} value of Pt(II) against $SKOV_3$ cells and $SKOV_3$DDP cells was 10.6 μmol/L and 24.4 μmol/L, respectively, the drug resistance index of $SKOV_3$DDP cells to Pt(II) was calculated to be 2.3. These results were positive related with the previously drug resistance index measured by MTT assay, indicating that $^{Cy5\text{-}miR}$NGO-PEG-FA probe could reflect the drug resistance degree with positive relationship.

The targeting ability of $^{Cy5\text{-}miR}$NGO-PEG-FA to tumor cells was evaluated by comparing the internalization of $^{Cy5\text{-}miR}$NGO-PEG-FA and $^{Cy5\text{-}miR}$NGO-PEG to folate receptor over expressed $SKOV_3$DDP cells. We observed the fluorescence signal in $SKOV_3$DDP cells after incubation at 37 °C for 30 min and 2 h, respectively (Fig. 3B and Fig. S11 in Supporting information). Obviously fluorescence signal was observed after NGO-PEG-FA was incubated with $SKOV_3$DDP cells at 37 °C for 30 min and 2 h, in contrast, almost no fluorescence was detected when $SKOV_3$DDP cells were incubated with $^{Cy5\text{-}miR}$NGO-PEG for 2 h, indicating that $^{Cy5\text{-}miR}$NGO-PEG-FA selectively targeted and internalized into the $SKOV_3$DDP cells. In order to further confirm the targeting ability was attributed to the folate, the $SKOV_3$DDP cells were previous treated with PEG-FA for 2 h before incubated with $^{Cy5\text{-}miR}$NGO-PEG-FA in order to block the folate receptors thus to hind the subsequent binding of $^{Cy5\text{-}miR}$NGO-PEG-FA. The result showed that no obvious intracellular fluorescence was observed when the folate receptors were blocked, indicating that the $^{Cy5\text{-}miR}$NGO-PEG-FA has tumor targeting ability.

To study whether the platform can enhance the uptake of Pt(IV) into tumor cells compared with the free Pt(IV) or Pt(II), the Pt uptake content into $SKOV_3$DDP cells was investigated, NGO-PEG-FA-Pt, free Pt(II) and free Pt(IV) were determined by ICP-OES (Fig. S12 in Supporting information), the results showed that the Pt uptake content of NGO-PEG-FA-Pt reached 42 pg/cell in 1 h incubation, which was significantly higher than the cellular uptake of Pt(II) or Pt(IV).

To further determine the capability of *let-7i* reverses drug resistance, the expression of cyclin D1 protein after miRNA *let-7i* transfection into $SKOV_3$DDP cells was measured by western blot. As shown in Fig. 4A, compared with NGO-PEG-FA, the protein expression level of cyclin D1 was significantly reduced in the $^{let\text{-}7i}$NGO-PEG-FA treated cells. cyclin D1 functions as a cyclin-dependent kinase C and its main function is to promote cell proliferation. It has been demonstrated that cyclin D1 imposes chemo-resistance on cancer cells [28]. *Let-7i* exerts an anti-chemo-resistance role through downregulation of cyclin D1 expression in $SKOV_3$DDP cells.

Finally, the biocompatibility of NGO was studied. No significant cytotoxicity was observed even when the concentration of NGO

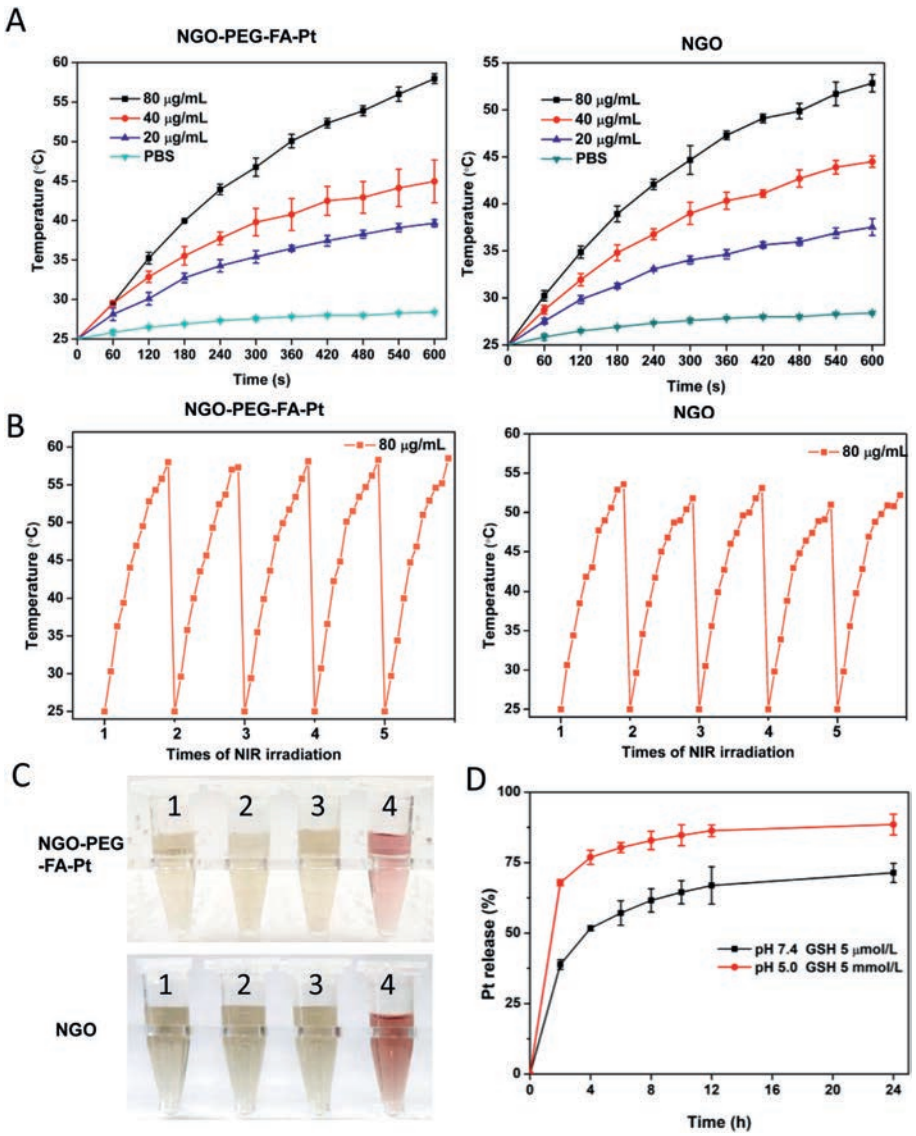

Fig. 2. (A) Temperature of NGO and NGO-PEG-FA-Pt solutions with different NGO content (20, 40, 80 μg/mL) for different times. (B) Temperature alternation of NGO and NGO-PEG-FA-Pt solutions (80 μg/mL) under NIR laser irradiation during the 5 "on-off" cycles (1.25 mg/mL, 1.03 W/cm^2). (C) Stability of NGO-PEG-FA-Pt and NGO in different mediums (1: PBS, 2: water, 3: MES, 4: RPMI medium containing 10% fetal bovine serum, respectively) after two weeks. (D) The release profile of Pt(II) from NGO-PEG-FA-Pt in PBS buffer at the condition of (pH 7.4 and GSH 5 μmol/L) or (pH 5.0 and GSH 5 mmol/L).

was increased to 200 μg/mL (Fig. S13 in Supporting information). With NIR laser irradiation, NGO showed a dose-dependent cytotoxicity from 1.56 μg/mL to 50 μg/mL (Fig. S14 in Supporting information). To conform that this platform has the chemical/photothermal synergetic therapy effects, we treated SKOV$_3$DDP cells with Pt(II), Pt(IV), NGO-PEG-FA-Pt, ^{miR}NGO-PEG-FA-Pt, FA/NGO-PEG-FA-Pt and ^{miR}NGO-PEG-FA-Pt/NIR with 808 nm laser irradiation at 1.5 W/cm^2 for 3 min, and compared their cell viability (Fig. 4B). Pt(II) and NGO-PEG-FA-Pt exhibited a dose-dependent cytotoxicity, with the IC_{50} values around 23.0 μmol/L and 12.2 μmol/L, respectively. It was worth noting that the ^{miR}NGO-PEG-FA-Pt displayed 3-fold higher activity than Pt(II) and reversed drug resistance, with the IC_{50} value being around 6.9 μmol/L. Moreover, the application of photothermal heating *via* 808 nm laser irradiation greatly increased the therapeutic efficacy of ^{miR}NGO-PEG-FA-Pt to SKOV$_3$DDP cells, resulting in a significant decrease of IC_{50} (0.4 μmol/L) after 48 h incubation. The heat production under laser irradiation is likely to make ^{miR}NGO-PEG-FA-Pt more potentially useful for the treatment of solid tumors with drug resistance. In order to further verify that the present of folate in the nanocomposite has target effect, the cytotoxicity of ^{miR}NGO-PEG-FA-Pt on folate saturated SKOV$_3$DDP cells was investigated. Low therapeutic effects were observed for all the concentrations of ^{miR}NGO-PEG-FA-Pt with the pre-treatment using folate, suggesting that the folate receptor-mediated endocytic pathway was blocked, thus the uptake of Pt(IV) and antitumor effect were reduced. To investigate the therapeutic efficiency of ^{miR}NGO-PEG-FA-Pt nanoparticles on SKOV$_3$DDP cells, calcein-AM/PI double staining experiment was conducted. Calcein-AM is a cell staining reagent for fluorescent labeling of living cells, which emits green fluorescence. PI can only entry the dead cells to produce red fluorescence. By comparing the proportion of green and red fluorescent cells, therapeutic efficiency between different treatments can be determined. As shown in Fig. 4C and Table S2 (Supporting information), the ^{miR}NGO-PEG-FA-Pt groups exhibited obvious red fluorescence, which confirmed that ^{miR}NGO-PEG-FA-Pt caused obvious damage on SKOV$_3$DDP cells. The cells treated by ^{miR}NGO-PEG-FA-Pt exhibited a higher percentage of red-stained cells (38.13%) than that of

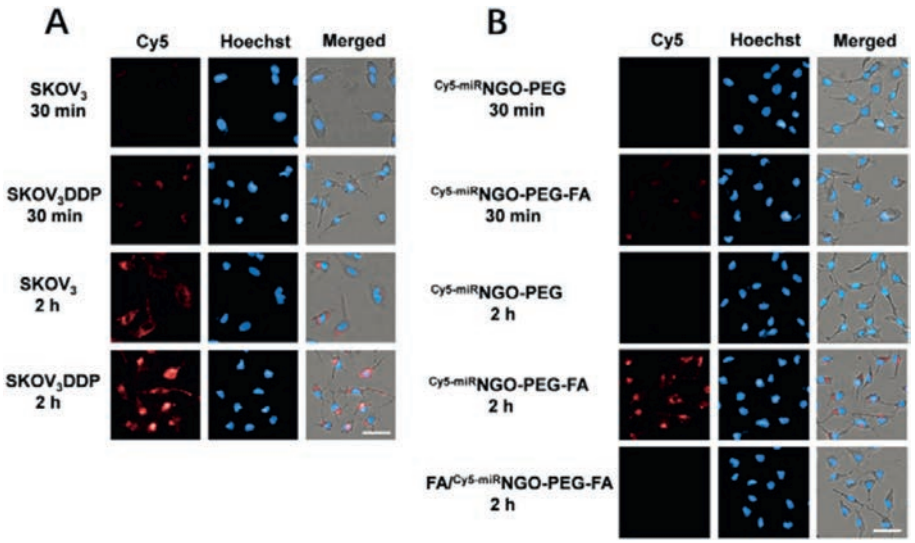

Fig. 3. (A) Fluorescence images of $SKOV_3$ and $SKOV_3$DDP cells incubated with $^{Cy5\text{-}miR}$NGO-PEG-FA for 30 min and 2 h (scale bar: 25 μm). (B) Fluorescence images of $SKOV_3$DDP cells incubated by $^{Cy5\text{-}miR}$NGO-PEG and $^{Cy5\text{-}miR}$NGO-PEG-FA for 30 min or 2 h (scale bar: 25 μm). For FA/$^{Cy5\text{-}miR}$NGO-PEG-FA group, cells were previously incubated with PEG-FA.

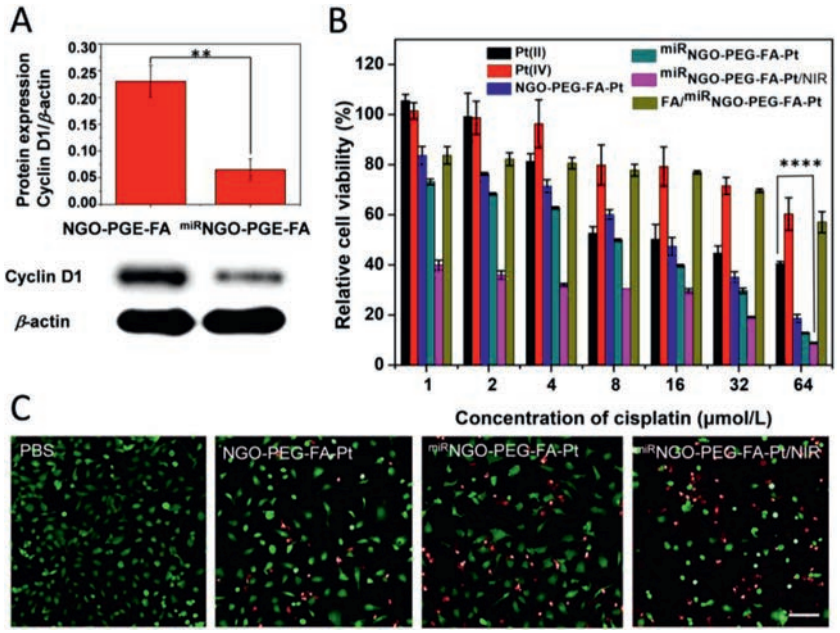

Fig. 4. (A) The suppression of cyclin D1 protein expression *via* ^{miR}NGO-PEG-FA. (B) Cell viability of $SKOV_3$DDP cells incubated with Pt(II), Pt(IV), NGO-PEG-FA-Pt(IV), ^{miR}NGO-PEG-FA-Pt, ^{miR}NGO-PEG-FA-Pt(IV)/NIR and FA/^{miR}NGO-PEG-FA-Pt at different concentrations of Pt from 1 μmol/L to 64 μmol/L for 48 h with or without NIR laser irradiation (1.5 W/cm^2, 3 min). For FA/^{miR}NGO-PEG-FA-Pt group, cells were previously incubated with PEG-FA. (C) $SKOV_3$DDP cells viability after different treatments *via* calcein-AM/PI double staining (scale bar: 50 μm).

the NGO-PEG-FA-Pt treated group (20.53%), this could be attributed to the reversal of drug resistance by miRNA (*let-7i*). In the ^{miR}NGO-PEG-FA-Pt/NIR group, the percentage of red-staining cells increased to about 52.80%. These results indicate that NIR laser irradiation significantly enhanced the therapeutic efficiency of ^{miR}NGO-PEG-FA-Pt.

In summary, an innovative multifunctional platform based on Pt(IV) and Cy5-miR loaded nano graphene oxide has been successfully prepared in this study, which detected/reversed intracellular drug resistance-related mRNA, as well as exhibited chemical-photothermal therapy. The NGO-PEG-FA could target to tumor cells *via* conjugated folate for active targeting and endocytosis, and the loaded Cy5-miR display capability of detecting intracellular drug resistance-related mRNA. Moreover, the miRNA *let-7i* suppressed the cyclin D1 protein expression to sensitize the role of NGO-PEG-FA-Pt in cytotoxicity. miRNAs simultaneously performed detection and treatment were seldom reported. In addition, the bio-responsive nanocomposite NGO-PEG-FA-Pt released Pt in responsive to acid and reductive environment enhanced its antitumor efficacy, and the photothermal properties of the NGO further increased the therapeutic effect of NGO-PEG-FA-Pt. Compared to cisplatin-based chemotherapy, $^{Cy5\text{-}miR}$NGO-PEG-FA-Pt nanocomposite showed excellent stability, higher drug uptake capacity and more efficient cisplatin-resistant carcinoma cellar cytotoxicity [29,30]. However, further understanding of the possible sub-organ transfer, clearance routes and potential toxicity of the

nanocarriers after intravenous injection still need to be explored. Based on the above results, we suggest that the multifunctional $^{Cy5\text{-}miR}$NGO-PEG-FA-Pt platform, combining detect/reverse of cancer drug resistance as well as synergistic therapeutic effects is promising for cancer treatment. Further in-depth work is likely to be done in the future to investigate this new type of drug delivery system.

Declaration of competing interest

The authors declare that they have no known competing financial interests or personal relationships that could have appeared to influence the work reported in this paper.

Acknowledgments

This work was supported by the Huxiang Young Talent Program of Hunan Province (No. 2018RS3005), the Innovation-Driven Project of Central South University (No. 2020CX048), the Changsha Science and Technology Plan Project (Nos. kq2005001, kq2004086), the National Natural Science Foundation of China (No. 81301258), the Natural Science Foundation of Hunan Province (Nos. 2019JJ60071, 2020JJ4680), the Shenghua Yuying Project of Central South University, the Hunan Provincial Graduate Research and Innovation Project (No. CX20190242), National College Students' Innovation and Entrepreneurship Training Program (Nos. S2020105330414, S202010533015X, 8304180412), the Postgraduate Innovation Project of Central South University (Nos. 2020zzts819, 2020zzts408, 2020zzts409, 2021zzts0977, 2021zzts0979), and the Open-End Fund for the Valuable and Precision Instruments of Central South University.

Supplementary materials

Supplementary material associated with this article can be found, in the online version, at doi:10.1016/j.cclet.2021.08.018.

References

[1] L. Kelland, Nat. Rev. Cancer 7 (2007) 573–584.
[2] Y.J. Huang, Y.F. He, Z.Y. Huang, Nanoscale 9 (2017) 10002–10019.
[3] X.Q. Quan, L. Rang, X.Z. Yin, Chin. Chem. Lett. 26 (2015) 695–699.
[4] H.B. Song, D.C. Liu, S.W. Dong, Signal Transduct. Tar. 5 (2020) 193.
[5] L.M. Crane, H.J. Arts, M. van Oosten, Cell Oncol. (Dordr) 35 (2012) 9–18.
[6] R.W. Robey, K.M. Pluchino, M.D. Hall, Nat. Rev. Cancer 18 (2018) 452–464.
[7] L. Galluzzi, L. Senovilla, I. Vitale, Oncogene 31 (2012) 1869–1883.
[8] A.E. Pasquinelli, B.J. Reinhart, F. Slack, Nature 408 (2000) 86–89.
[9] T. Yang, P.X. Zhao, Z. Rong, Theranostics 6 (2016) 142–154.
[10] L. Elkhadragy, M.Y. Chen, K. Miller, Mol. Oncol. 11 (2017) 194–207.
[11] K. Liu, T. Qian, L. Tang, World J. Surg. Oncol. 10 (2012) 225.
[12] X. Li, T. Liang, S.S. Chen, J. Cell. Biochem. 121 (2020) 2139–2149.
[13] Y. Zhang, R. Zhu, J. Wang, Artif. Cell. Nanomed. Biotechnol. 47 (2019) 3854–3861.
[14] B.C. de Almeida, L.G. dos Anjos, M. Uno, Cells 8 (2019) 1452.
[15] N. Yang, S. Kaur, S. Volinia, Cancer Res. 68 (2008) 10307–10314.
[16] Z. Liu, B. Liu, J. Ding, Anal. Bioanal. Chem. 406 (2014) 6885–6902.
[17] Q. He, Q. Wu, X. Feng, Int. J. Biol. Macromol. 151 (2020) 757–780.
[18] Y. Wang, J. Yan, N. Wen, Biomaterials 230 (2020) 119619.
[19] Y. Hu, Y. Wang, J. Yan, Adv. Sci. (Weinh) 7 (2020) 2000557.
[20] Y. Wang, Y. Hu, Q. He, Biosens. Bioelectron. 169 (2020) 112604.
[21] W.Q. Yu, M. Shevtsov, X.C. Chen, Chin. Chem. Lett. 31 (2020) 1366–1374.
[22] Z. Liu, S. Chen, B. Liu, Anal. Chem. 86 (2014) 12229–12235.
[23] F. He, N. Wen, D. Xiao, Curr. Med. Chem. 27 (2020) 2189–2219.
[24] J. Yan, H. Xiong, S. Cai, Talanta 200 (2019) 124–144.
[25] T.K. Mandal, Y.R. Lee, N. Parvin, Biomater. Sci. 8 (2019) 125–131.
[26] C.M. Ma, J.L. Zhang, Y. Zhang, Chin. Chem. Lett. 32 (2021) 1550–1554.
[27] P. Du, J. Yan, S. Long, J. Mater. Chem. B 8 (2020) 4046–4055.
[28] L. Elkhadragy, M. Chen, K. Miller, Mol. Oncol. 11 (2017) 194–207.
[29] Q.L. Chen, Y.Y. Yang, X. Lin, Chem. Commun. 54 (2018) 5369–5372.
[30] W. Zhang, J.L. Shen, H. Su, ACS Appl. Mater. Interfaces 8 (2016) 13332–13340.